LRR protein RNH1 inhibits inflammasome activation through proteasome-mediated degradation of Caspase-1 and is associated with adverse clinical outcomes in COVID-19 patients.

Giuseppe Bombaci[1,2,3,12], Mayuresh Anant Sarangdhar[1,2,12], Nicola Andina[1,2,], Aubry Tardivel[1,2], Eric Chi-Wang Yu[4], Gillian M. Mackie[5,6], Matthew Pugh[5], Vedat Burak Ozan[2,1], Yara Banz[7], Thibaud Spinetti[8], Cedric Hirzel[9], Esther Youd[10], Joerg C. Schefold[8], Graham Taylor[5], [1], Amiq Gazdhar[2,11], Nicolas Bonadies[1,2], Anne Angelillo-Scherrer[1,2], Pascal Schneider[4], Kendle M. Maslowski[5,6], Ramanjaneyulu Allam[1,2,13]

Affiliations:

1.Department of Hematology and Central Hematology Laboratory, Inselspital, Bern University Hospital, University of Bern, Switzerland.

2.Department for BioMedical Research, University of Bern, Switzerland.

3.Graduate School for Cellular and Biomedical Sciences, University of Bern, Bern, Switzerland.

4.Department of Biochemistry, University of Lausanne, Lausanne, Switzerland.

5.Institute of Immunology and Immunotherapy, University of Birmingham, Birmingham, UK.

6. Institute of Metabolism and Systems Research, University of Birmingham, Birmingham, UK.

7. Institute of Pathology, University of Bern, Switzerland.

8.Department of Intensive Care Medicine, Inselspital, Bern University Hospital, University of Bern, Switzerland.

9. Department of Infectious Diseases, Inselspital, Bern University Hospital, University of Bern, Switzerland.

10. School of Medicine, Dentistry & Nursing, Forensic Medicine and Science. University of Glasgow.

11.Department of Pulmonary Medicine, Inselspital, Bern University Hospital, University of Bern, Switzerland.

12. These authors contributed equally

13. Lead contact

***Correspondence:**

Ramanjaneyulu Allam, PhD
Department of Hematology and Central Hematology Laboratory,
Inselspital, Bern University Hospital,
Department for BioMedical Research, University of Bern,
Murtenstrasse 40, CH-3008 Bern, Switzerland.
Phone: +41-31 632 7753
Email: allam.ramanjaneyulu@dbmr.unibe.ch
orcid.org/0000-0002-2789-3596

SUMMARY

Inflammasomes are cytosolic innate immune sensors that, upon activation, induce caspase-1 mediated inflammation. Although inflammation is protective, uncontrolled excessive inflammation can cause inflammatory diseases and is also detrimental in COVID-19 infection. However, the underlying mechanisms that control inflammasome activation are incompletely understood. Here we report that the leucine rich repeat (LRR) protein Ribonuclease inhibitor (RNH1), which shares homology with LRRs of NOD-like receptor family pyrin domain (PYD)-containing (NLRP) proteins, attenuates inflammasome activation. Mechanistically, RNH1 decreased pro-IL1β expression and induced proteasome-mediated caspase-1 degradation. Corroborating this, mouse models of monosodium urate (MSU)-induced peritonitis and LPS-induced endotoxemia, which are dependent on caspase-1, respectively showed increased neutrophil infiltration and lethality in *Rnh1*$^{-/-}$ mice compared to WT mice. Further, RNH1 protein levels were negatively correlated with inflammation and disease severity in hospitalized COVID-19 patients. We propose that RNH1 is a new inflammasome regulator with relevance to COVID-19 severity.

KEYWORDS: Ribonuclease Inhibitor-1 (RNH1), Inflammasomes, NLRP3, COVID-19, SARS-CoV-2, Inflammation, LRR protein, NF-κB and negative regulator of inflammation.

INTRODUCTION

Innate immune receptors sense invading pathogens or endogenous danger molecules that are released by dying cells and induce inflammation, which is critical to eliminate pathogens and to initiate tissue repair (Gong et al., 2020). Inflammasomes are cytosolic innate immune receptors that upon activation form multiprotein caspase-1-activating complexes containing an adaptor protein ASC (apoptosis-associated speck-like protein containing a caspase activation and recruitment domain) and caspase-1 (Martinon et al., 2009; Schroder and Tschopp, 2010). Active caspase-1 processes the IL-1 cytokine members IL-1β and IL-18 and initiates Gasdermin-D (GASMD)-mediated pyroptosis, a form of cell death (Broz and Dixit, 2016). Several NOD-like receptor (NLRs) proteins, as well as HIN200 proteins and Pyrin, can form inflammasome complexes, namely: NLR family pyrin domain (PYD)-containing 1 (NLRP1), NLRP3, NLRP6, NAIP/NLRC4, AIM2 and Pyrin (Broz and Dixit, 2016; Schroder and Tschopp, 2010). The NLR family is characterized by the presence of a central nucleotide-binding and oligomerization (NACHT) domain, which is commonly flanked by C-terminal leucine-rich repeats (LRRs) and N-terminal CARD or pyrin (PYD) domains. LRRs are believed to function in ligand sensing and autoregulation, whereas CARD and PYD domains mediate homotypic protein-protein interactions for downstream signaling. Inflammasomes are activated after sensing host-derived danger-associated molecular patterns (DAMPs), bacterial toxins, nucleic acids, pathogenic crystals, and altered cellular components (Gong et al., 2020; Henao-Mejia et al., 2014).

Inflammasomes are critical to mount immune responses, however uncontrolled inflammasome activation is associated with several autoimmune and inflammatory diseases including Coronavirus disease 2019 (COVID-19) (Strowig et al., 2012; van den Berg and Velde, 2020). COVID-19 caused by severe acute respiratory syndrome coronavirus 2 (SARS-CoV-2) is associated with significant mortality and has resulted in more than 2

million deaths worldwide until now. Clinical manifestation of patients with COVID-19 include pulmonary failure including acute respiratory distress syndrome (ARDS) and cardiac injury (Huang et al., 2020a). Several studies suggest that overproduction of proinflammatory cytokines correlates with increased disease severity and poor prognosis in hospitalized COVID-19 patients (Jose and Manuel, 2020; Lucas et al., 2020; Mehta et al., 2020). In this line, recent studies reported inflammasome activation in severe COVID-19 patients and suggested that increased inflammasome activation would potentially mediate disease progression in COVID-19 (Kroemer et al., 2020; Rodrigues et al., 2021; Toldo et al., 2020; van den Berg and Velde, 2020). It is therefore important to understand molecules that control and resolve the overactivation of inflammasomes and inflammation in order to develop therapeutic targets for COVID-19 and other inflammatory disorders.

Ribonuclease inhibitor (RNH1/RI), also known as Ribonuclease/Angiogenin Inhibitor, is a LRR protein (Dickson et al., 2005). It is present in the cytosol but can also be found in the nucleus and mitochondria (Furia et al., 2011). The known function of RNH1 is to bind to pancreatic-type ribonucleases with femtomolar affinity and render them inactive (Dickson et al., 2005). In addition, several roles of RNH1 have been reported such as inhibiting oxidative damage (Dickson et al., 2005; Monti et al., 2007), inhibiting angiogenin (ANG) mediated neovascularization and stemness of haematopoietic stem cells (Dickson et al., 2009; Goncalves et al., 2016), binding and inhibition of ER stress sensor IRE1 activity (Tavernier et al., 2018), inhibiting of tiRNA degradation (Yamasaki et al., 2009), and mediate resistance to histone deacetylase inhibitor toxicity in cancer cell lines (Zhu et al., 2013). However, the relevance of these observations *in vivo* still needs to be validated. We recently reported that RNH1 is important for embryonic erythropoiesis in mice, suggesting possible additional roles for RNH1 in mammalian physiology (Chennupati et al., 2018). RNH1 was the first cytosolic protein identified to possess LRRs (Dickson et al., 2005). The

LRRs are present in a large family of proteins that display of vast surface areas to foster protein-protein and protein–ligand interactions (Kobe and Deisenhofer, 1993). LRR proteins are classified into subfamilies based on the organism of origin, cellular localization, LRR consensus sequence and length. To date, seven LRR subfamilies of proteins have been described: bacterial, ribonuclease inhibitor–like, cysteine-containing, SDS22, plant-specific, typical, and small (Dickson et al., 2005; Kobe and Kajava, 2001; Matsushima et al., 2010). Interestingly, members of the RNH1-like subfamily are intracellular proteins and include human MHC class II transactivator (CIITA), Ran GTPase activating protein from Saccharomyces pombe (RANGAP1), and other NLRs (Dickson et al., 2005). Further, the LRRs of RNH1 are very similar to those of NLRP proteins (Ng et al., 2011). Whether RNH1 plays a role in NLRP inflammasome activation is currently unclear.

In this study, we investigated the role of RNH1 in inflammation and found that RNH1 inhibits inflammasome activation by proteasome-mediated degradation of the downstream effector molecule caspase-1. Supporting this, *Rnh1*$^{-/-}$ mice displayed higher inflammasome-dependent activation of caspase-1. Interestingly, we also found that RNH1 expression in buffy coat and lung biopsies negatively correlated with SARS-CoV-2-mediated inflammation and severety in COVID-19 patients. Collectively, these findings establish RNH1 as a previously unidentified negative regulator of inflammasome activation, which might play a role in human inflammatory diseases including SARS-CoV-2 mediated inflammation and pathology.

RESULTS

RNH1 is predominantly expressed in myeloid cells and is increased under inflammatory conditions.

Human RNH1 protein consists of 15 LRR repeats whose sequence and organization are similar to those present in multiple NLRP proteins (**Figure 1A)** (Hoss et al., 2019; Ng et al., 2011). RNH1 consists exclusively of LRRs and lacks functional domains present at the N.-terminus of NLRP proteins (**Figure 1B)**. LRRs in NLRP family proteins are believed to function in ligand sensing and autoregulation (Schroder and Tschopp, 2010). Since NLRPs form inflammasome complexes and induce inflammation, we investigated the role of RNH1 in inflammasome activation. We stained healthy human bone marrow biopsies for RNH1 and found that RNH1 is expressed at higher levels in myeloid cells compared to other hematopoietic cell types such as lymphocytes and erythrocytes (**Figure 1C**). Further, RNH1 protein expression is elevated in bone marrow biopsies of patients with confirmed systemic inflammation (see methods) (**Figure 1D).** In support of this observation, RNH1 protein levels in human monocyte cell line (THP1 cells) and primary mouse bone marrow derived macrophages (BMDM) were moderately increased upon stimulation with the TLR1/2 ligand Pam3Cysk4 and the TLR4 ligand LPS, respectively (**Figure 1E and F**). Collectively, these results suggest that RNH1 is predominantly expressed in myeloid cells and might play a role in inflammation.

Absence of RNH1 increases NLRP3 inflammasome activation

The NLRP3 inflammasome is the most studied and is activated by several pathogens as well as danger stimuli (Broz and Dixit, 2016). To investigate the role of RNH1 in NLRP3 inflammasome activation, we generated RNH1-deficient (RNH1-KO) THP1 cells using the CRISPR/cas9 system and stimulated them with NLRP3 agonists. RNH1-KO THP1 cells showed increased mature IL-1β production and caspase-1 cleavage compared to wildtype

cells (**Figure 2A and 2B**). shRNA knockdown studies in THP1 also showed similar results (**Supplementary Figure 1A and B).** Since human and mouse RNH1 share 72.8% homology at the protein level, we also checked NLRP3 activation in mouse-derived immortalized macrophages (iMAC cells). RNH1-KO iMAC cells also showed increased caspase-1 cleavage and mature IL-1β production in response to NLRP3 agonists (**Figure 2C and 2D**). This data suggests that RNH1 limits inflammasome activation in both human and mouse. Inflammasome activation triggers pyroptosis, a type of inflammatory cell death (Miao et al., 2011). We indeed observed increased cell death in RNH1-KO cells compared to WT cells upon NLRP3 activation (**Figure 2E and 2F**). In order to confirm the inhibitory function of RNH1 on inflammasome activation, we performed a transient reconstitution of RNH1 in RNH1-KO THP1 cells using lentiviral transduction, followed by stimulation with NLRP3 agonists. Reconstitution of RNH1 caused a decrease in IL-1β secretion (**Figure 2G and 2H**). Further, we also generated stable RNH1 over-expressing THP1 cells and stimulated them with NLRP3 agonists. RNH1 overexpression decreased IL-1β secretion confirming that RNH1 negatively regulates NLRP3 inflammasome activation (**Figure 2I and 2J**). In line with increased NLRP3 inflammasome activation, RNH1-KO THP1 cells also showed enhanced ASC speck formation upon nigericin stimulation, which is a direct indicator of inflammasome activation (Stutz et al., 2013) (**Figure 2K and 2L**). Collectively, these results suggest that RNH1 dampens NLPR3 inflammasome activation.

RNH1 regulates NF-kB activation and is involved in the priming of NLRP3

Activation of the canonical NLRP3 inflammasome activation occurs in two steps (Latz et al., 2013). The priming step requires activation of nuclear factor kappa B (NF-κB), *e.g.* when LPS binds to TLR4, which upregulates NLRP3 and pro-IL-1β. The second step requires a signal initiated by pathogen-associated molecular patterns (PAMPs) or DAMPs, which leads to NLRP3 activation and formation of an inflammasome complex with ASC and Caspase-1

(Latz et al., 2013). We found increased pro-IL-1β in RNH1-KO cells suggesting that RNH1 might also be involved in reducing the priming signal (**Figure 2B and 2D**). To further understand this, wildtype and RNH1-KO THP1 cells were stimulated with the TLR2 ligand Pam3CSK4. RNH1-KO cells showed increased pro-IL-1β and NLRP3 expression in both time- and Pam3CSK4 concentration-dependent manner, supporting a role of RNH1 in priming, (**Figure 3A and 3B**). RNH1-KO cells displayed increased NF-κB p100 activation at 40, 60 and 180 min after Pam3CSK4 treatment (**Figure 3C**). In addition, they also showed decreased levels of the IκBα and increased levels of phospho-IκBα compared to wildtype cells (**Figure 3C).** To further confirm NF-κB activation, we monitored the production of pro-inflammatory cytokines and found that RNH1-KO cells exhibited enhanced secretion of TNF and IL-6 compared to wildtype cells (**Figure 3D and E).** Collectively, these results suggest that RNH1 reduces NF-κB activation and therefore reduces the priming step.

RNH1 deficiency increases AIM2 and NAIP/NLRC4 inflammasome activation

To check whether RNH1 is also involved in activation of AIM2 and NAIP/NLRC4 inflammasomes, we stimulated wildtype and RNH1-KO THP1 cells with cytosolic dsDNA (pdA:dT) and flagellin, respectively. Interestingly, we found increased mature IL-1β production and caspase-1 cleavage in RNH1-KO compared to wildtype cells (**Figure 3F and 3G**), suggesting increased AIM2 and NAIP/NLRC4 inflammasome activation in RNH1-KO THP1 cells. We also found increased AIM2 inflammasome activation in mouse iMAC cells, however there was no significant increase in cytosolic flagellin-induced NAIP/NLRC4 inflammasome activation (**Figure 3H and 3I**). To further confirm the inflammasome activation, we checked ASC oligomerization by monitoring the partition of ASC in insoluble fractions (Lugrin and Martinon, 2017). In line with the above results, loss of RNH1 increased ASC oligomerization in response to NLRP3 and AIM2 inflammasome activators (**Supplementary Figure 2A**). We also found increased cell death in RNH1-KO cells by

AIM2 activation (**Supplementary Figure 2B and 2C**). Together, these results suggest that loss of RNH1 also negatively regulates AIM2 and NAIP/NLRC4 inflammasome activation.

RNH1 mediates degradation of caspase-1 through the proteasome

Since RNH1 inhibits the activation of several inflammasomes (NLRP3, AIM2 and NAIP/NLRC4), it could do so by acting on a common downstream effector. Interestingly, caspase-1 protein levels were elevated in RNH1-KO cells at steady state (**Figure 4A**). A qPCR analysis indicated that RNH1 does not regulate caspase-1 at the transcriptional level (**Figure 4B)**. To check whether RNH1 regulate caspase-1 expression at the translation or post-translational levels, we performed chase experiments using actinomycin-D, cycloheximide (CHX) and the proteasome inhibitor MG-132 in wildtype and RNH1-KO THP1 cells. Actinomycin-D and CHX inhibits transcription and translation respectively. Actinomycin-D and CHX treatment decreased caspase-1 protein levels in both wildtype and RNH1-KO cells with similar kinetics **(Figure 4C and D)**. Interestingly, proteasome blockade with MG-132 increased caspase-1 protein levels in WT cells while levels were not further increased in RNH1-KO cells, suggesting that loss of RNH1 might stabilize caspase-1 protein levels by inhibiting proteasome mediated degradation **(Figure 4E)**. To test this further, we expressed full length Flag-caspase-1 in the presence or absence of GFP-RNH1 in HEK293T cells. Strikingly, caspase-1 protein levels decreased with increasing concentration of RNH1, an effect that was blocked in the presence of MG-132 **(Figure 4F)**. It has been reported that overexpression of caspase-1 induces self-cleavage (Li et al., 2008), however, we did not observe caspase-1 self-cleavage at the concentration that we used in our experiments. Interestingly, we also did not observe a similar decrease in another protease, OMI/HTRA2 (Vande Walle et al., 2008) in the presence of RNH1 **(Figure 4G)**, suggesting that RNH1 might specifically mediate proteasomal degradation of caspase-1 or of a defined set of proteins. Since proteins must be ubiquitinated for proteasome mediated

degradation, we checked caspase-1 ubiquitination (Ub) in wildtype and RNH1-KO THP1 cells by immunoprecipitating ubiquitin. Interestingly, the ratio of poly-Ub-caspase-1 and total caspase-1 levels were decreased in RNH1-KO cells **(Figure 4H and I),** suggesting that absence of RNH1 might decrease caspase-1 ubiquitination. We attempted to co-express HA-tagged ubiquitin and caspase-1 in the presence or absence of RNH1 in HEK293T cells. However, in the presence of RNH1, caspase-1 was found to be completely degraded, so we could not study caspase-1 ubiquitination in the presence of RNH1 (data not shown). Collectively, these results suggest that RNH1 increases proteasome-mediated caspase-1 degradation, possibly through controlling ubiquitination of caspase-1.

Loss of RNH1 in mice increases inflammation and lethality upon inflammasome activation

Complete deletion of *Rnh1* leads to embryonic lethality in mice (Chennupati et al., 2018), so we generated *Rnh1* conditional knockout mice (*Rnh1*$^{fl/fl}$) to understand the *in vivo* relevance of our results (**Figure 5A)**. We crossed *Rnh1*$^{fl/fl}$ mice with transgenic interferon-inducible *Mx1-Cre* mice to generate an inducible *Rnh1*$^{-/-}$ mouse model (*Rnh1* $^{fl/f;Mx1\text{-}Tg+}$). Administration of polyinosinic:polycytidylic acid (polyI:C) into *Rnh1*$^{fl/f;Mx1\text{-}Tg+}$ mice lead to cre-recombination and complete deletion of RNH1 protein expression in hematopoietic organs such as the bone marrow (BM), which we refer to as *Rnh1*$^{-/-}$ (**Figure 5B and C**). We generated BM-derived macrophages (BMDM) from WT (*Rnh1*$^{fl/fl}$) and *Rnh1*$^{-/-}$ mice and stimulated them with inflammasome activators. As seen above in cell lines, loss of RNH1 in primary mouse BMDMs lead to increased mature IL-1β production and caspase-1 cleavage compared to wildtype cells upon stimulation with NLRP3, AIM2 and NAIP/NLRC4 agonists (**Figure 5D and E**). To check the *in vivo* role of Rnh1 in inflammasome activation, we performed mouse models of caspase-1-dependent MSU-induced peritonitis and LPS-induced lethality mouse models (Li et al., 1995; Man et al., 2017; Martinon et al., 2006)

(**Figure 5F**). Since *Mx1-Cre* activation also deletes genes in non-haematopoietic organs (Kühn et al., 1995), we transplanted WT (*Rnh1*$^{fl/fl}$) and *Rnh1*$^{-/-}$ (*Rnh1*$^{fl/fl}$ *Mx1-Cre*$^{+}$) bone marrow into irradiated CD45.1 congenic mice to exclude Rnh1 effects from non-hematopoietic cells. After 8 weeks we checked reconstitution levels in WT and *Rnh1*$^{-/-}$ BM transplanted CD45.1 congenic mice. We found comparable reconstitution in WT and *Rnh1*$^{-/-}$ BM transplanted CD45.1 congenic mice **(Figure 5G).** *Rnh1* was deleted by giving three rounds of 200 µg of polyI:C injections. Four days after the last injection mice were analyzed for peripheral blood parameters. At this time point, we observed no major difference in leukocyte numbers **(Figure 5H)**, hemoglobin and red blood cell count (data not shown) between WT and *Rnh1*$^{-/-}$ BM transplanted CD45.1 congenic mice. In a MSU-induced model of peritonitis, *Rnh1*$^{-/-}$ mice showed increased neutrophil infiltration in the peritoneal cavity compared to WT mice (**Figure 5I).** Consistent with this, we also found increased IL-1β production in the peritoneal lavage of *Rnh1*$^{-/-}$ mice compared to WT mice **(Figure 5J).** We next challenged mice with LPS at 10 mg/kg, a dose that killed *Rnh1*$^{-/-}$ mice but not WT mice that all survived this dose of LPS **(Figure 5K)**. Altogether, these results demonstrate that *Rnh1* deficiency promotes excessive inflammasome activation and increases inflammation.

RNH1 is negatively associated with disease severity in COVID-19 patients

Recent studies suggest that pronounced inflammation and inflammasome activation in patients with COVID-19 correlates with increased disease severity and poor prognosis (Ferreira et al., 2021; Jose and Manuel, 2020; Kroemer et al., 2020; Lucas et al., 2020; Mehta et al., 2020; Rodrigues et al., 2021; Toldo et al., 2020; van den Berg and Velde, 2020). Since our results suggest that RNH1 negatively regulates NFκB and inflammasome activation, we investigated RNH1 levels in COVID-19 patients. Buffy coat samples from critically ill COVID-19 patients admitted to the intensive care unit (ICU) (n= 17) and COVID-19 patients admitted to general COVID-19 ward (n=11 patients) were analyzed for RNH1 protein

expression by western blot (see methods). Disease severity of these patients is estabilished by comorbidity data and routine clinical parameters, such as C-reactive protein **(Supplementary Table 1).** Strikingly, ICU COVID-19 patients had significant less RNH1 expression when compared to general ward COVID-19 patients (**Figure 6A,B and Supplementary Figure 3).** The decrease of RNH1 expression in ICU patients is unlikely to reflect leukocyte numbers, since leukocyte numbers were ranther increased in ICU patients compared to general ward COVID-19 patients **(Supplementary Table 1).** To further support these findings, we analyzed RNH1 expression with an anti-RNH1 antibody in lung sections of patients from an independent study performed in the UK, who deceased either from COVID-19 (n = 6) or from non-viral causes (n =11) (.**Supplementary Table 1).** In line with the data above, RNH1 expression is largely absent in lungs of deceased COVID-19 patients, whereas patients having succumbed to non-viral causes do show RNH1 staining in infiltrating cells in the lung **(Figure 6C and Supplementary Figure 4)**. These data show loss of RNH1 expression in immune cells during severe COVID-19, which may suggest a crucial role for RNH1 in controlling severe inflammation.

Recent studies document the critical role for monocytes and macrophages in SARS-CoV-2 infection (Desai et al., 2020; Ferreira et al., 2021). To check whether RNH1 affects SARS-CoV-2 infection rate in macrophages, we infected WT and RNH1-KO macrophages differentiated from THP1 monocytes with SARS-CoV-2 pseudoviral particles (Hoffmann et al., 2020; Nie et al., 2020). These pseudoviral particles express SARS-CoV-2 spike protein together with enhanced GFP (eGFP) as a reporter. Interestingly, we found increased eGFP+ cells in RNH1-KO cells compared to WT cells (**Figure 6D)**. At a multiplicity of infection (MOI) of 0.25, we observed 1% of RNH1-KO cell were positive for eGFP cells. This increased to 2.5% at an MOI of 1, however we did not find any eGFP+ cells in the WT at

0.25 MOI and very few (<0.5%) at 1MOI. These results suggest that RNH1-KO cells are more susceptible to infection (**Figure 6D)**. Collectively, our findings suggest that decreased expression of RNH1 strongly correlates with severity and increased inflammation in COVID-19 patients, and possibly increases the risk of SARS-CoV-2 infection.

DISCUSSION

Inflammasomes are multiprotein cytoplasmic complexes which, upon activation, induce potent inflammation and gasdermin-D-mediated pyroptosis (Broz and Dixit, 2016). This process is critical for pathogen clearance and to maintain tissue homeostasis. However, uncontrolled inflammasome activation leads to excessive inflammation and tissue destruction, which is a prime cause for several inflammatory, autoimmune and autoinflammatory diseases (Lamkanfi and Dixit, 2011; Strowig et al., 2012). Therefore, precise regulation of inflammasome signaling is necessary to prevent collateral damage but still prevent pathogen insurgence. Our results unravel a new mechanism involving RNH1 acting as a negative regulator of inflammasome activation. Conventionally, RNH1 is known to inhibit ribonucleases and protect RNA from degradation (Dickson et al., 2005). However, in *Rnh1*-ko mice that are embryonically lethal because of marked defects in erythropoiesis, the defect seems to originate from decreased translation of the transcriptional erythropoiesis regulator GATA-1 rather than detectable effects on mRNA levels, suggesting that RNH1 fulfills functions beyond inhibition of ribonucleases (Chennupati et al., 2018). This is also supported by the present study in which RNH1 mainly exerts post-translational effects.

The RNH1 protein consists of only LRRs and evolved via exon duplication (Haigis et al., 2002). Interestingly, LRRs of RNH1 share homology with the LRRs of NLRs, yet the function of RNH1 in NLR signaling is not known. Although, RNH1 is a ubiquitously expressed protein (Dickson et al., 2005), we demonstrated that it is highly expressed in

myeloid cells and its expression is increased under inflammatory conditions, pointing to a potential role in regulating inflammation. Interestingly, we found that RNH1-deleted macrophages increased IL-1β production, caspase-1 activation and pyroptosis in response to NLRP3 agonists, suggesting that RNH1 can potentially inhibit NLRP3-induced inflammation. Increased expression of RNH1 in inflammatory conditions might be a compensatory mechanism to dampen inflammation. In addition, we identified increased NF-κB signaling and also increased expression of pro-IL-1β and NLRP3 expression in the absence of RNH1, which clearly indicates that RNH1 regulates NLRP3 inflammasome activation at the priming step as well as during the activating signal. We did not investigate mitogen-activated protein kinase (MAPK) pathways, which play a role in TLR induced inflammation (Arthur and Ley, 2013), so we cannot exclude that the MAPK pathway may mediated priming in RNH1-deleted cells. A report suggests that reactive oxygen species (ROS) are involved both in priming and in NLRP3 inflammasome activation (Zhou et al., 2010). RNH1 protein contains numerous cysteine residues (e.g. 32 in human RNH1), whose sulfhydryl groups might play a structural role and were also shown to protect from oxidative damage (Cui et al., 2003; Dickson et al., 2005). Thus, increased ROS production in the absence of RNH1 might be responsible for NLRP3 inflammasome activation. However, loss of RNH1 also increased AIM2 and NAIP/NLRC4 inflammasome activation, which do not require ROS. Therefore, these observations do not substantiate a major anti-ROS role of RNH1 to suppress activation of the NLRP3 inflammasome. Further studies are necessary to exclude a role of ROS in RNH1-mediated NLRP3 inflammasome regulation. Taken together, our data define RNH1 as an inhibitor of inflammasome activation. Whether RNH1 also inhibits non-canonical inflammasomes remains to be studied.

In line with the increased canonical inflammasome activation and higher caspase-1 activity in RNH1-KO cells, we observed higher caspase-1 protein levels in RNH1-KO cells compared to WT. Caspase-1 is a cysteine protease acting downstream of inflammasome activation. Upon activation, pro-caspase-1 is cleaved into two subunits (p10 and p20) and mediates proteolytic processing of pro-IL-1β and pro-IL-18 while promoting pyroptosis by cleaving gasdermin (Broz and Dixit, 2016). Few studies report mechanisms for the inhibition of caspase-1 function. Flightless-I binding could inhibit caspase-1 cleavage (Jin et al., 1AD; Li et al., 2008) and CARD only protein -1 (COP-1) was also shown to interact with the CARD domain of caspase-1 and inhibit caspase-1 interaction with ASC (Druilhe et al., 2001; Pedraza-Alva et al., 2015). However, to our knowledge, regulation of caspase-1 protein levels as found in the present study were not previously reported. Further, we demonstrated that RNH1 promotes proteasome-mediated caspase-1 protein degradation, which was rescued by inhibiting proteasome function. How RNH1 regulates proteasome-mediated caspase-1 degradation requires further investigation, but we did observe reduced ubiquitination of caspase-1 in the absence of RNH1. Caspase-1-deficient mice are resistant to LPS-induced lethality and MSU-induced peritonitis (Man et al., 2017; Martinon et al., 2006). Supporting a role for RNH1 in inflammasome activation and caspase-1 activity, *Rnh1*$^{-/-}$ mice showed markedly increased susceptibility to LPS-induced lethality. Further, *Rnh1*$^{-/-}$ mice also displayed increased neutrophil infiltration in MSU-induced peritonitis. These results mirror results obtained *in vitro*. Collectively, our study unravels a significant role of RNH1 in dampening inflammasome activation and demonstrates a previously unidentified regulation of caspase-1 through proteasome-mediated degradation (**Figure 6E**).

Uncontrolled inflammation mediates immune pathology in several inflammatory diseases including pandemic COVID-19 (Huang et al., 2020b; Jose and Manuel, 2020; Mehta et al.,

2020). Recent studies have demonstrated a correlation of increased inflammasome activation and disease severity in COVID-19 patients (Toldo et al., 2020; van den Berg and Velde, 2020). We showed that RNH1-KO THP1 cells are susceptible to infection with SARS-CoV-2 pseudo virus. Further, we identified a significant decrease in RNH1 protein expression in severe ICU-admitted COVID-19 patients compared to less severe general ward-admitted COVID-19 patients, suggesting that RNH1 expression negatively correlates with COVID-19 disease severity. This is contrary to what we have shown in inflammatory conditions, where increased RNH1 expression might be a compensatory mechanisms to inhibit inflammation (**Figure 1D)**. So it is unclear what drives the reduced expression of RNH1 in severe COVID-19 pathology, but understanding whether this is a common feature of severe inflammation, or of infection-driven inflammation, and what causes it will be of interest. In addition, these results were confirmed in an independent COVID-19 patient cohort using post-mortem lung tissue. We observed decreased RNH1 protein expression in COVID-19 lung sections compared to lungs from patients who died of non-viral causes.

These results have direct clinical implication. First, RNH1 expression in blood samples could be used as a marker for disease severity in COVID-19 patients, and potentially other inflammatory conditions including sepsis. Second, small molecules or drugs that could enhance RNH1 expression might be beneficial for COVID-19 and other inflammatory disease patients. Overall, the *in vitro* as well as *in vivo* mouse models along with human clinical data strongly suggest a potentially important role for RNH1 in limiting severe inflammation.

ACKNOWLEDGEMENTS

We thank Fabio Martinon, University of Lausanne for helpful discussions. We thank the

FACS and microscopy facility of the DBMR (University of Bern) for assistance in flow cytometry and confocal experiments, respectively. This work was supported by the Swiss National Science Foundation (PP00P3_157486, PP00P3_183721 & PP00P3_190073) to RA.

AUTHOR CONTRIBUTIONS

GB, MAS, NA, KMM, CHY performed experimental work. AT maintained mouse lines and helped with experimental work. NB and YB helped with histopathology of Human bone marrow samples.AG and VBO helped with COVID-19 pseudovirus infection studies. TS,CH and JCS provided COVID-19 patients samples and data. KMM, GM, MP, EY and GT helped with histopathology of COVID-19 lung biopsy data from UK. AAS and PS helped with reagents and advice. RA designed, supervised the research work and wrote the manuscript with inputs from all the authors.

DECLARATION OF INTERESTS

All the authors declare no competing interests to this work

MAIN FIGURES

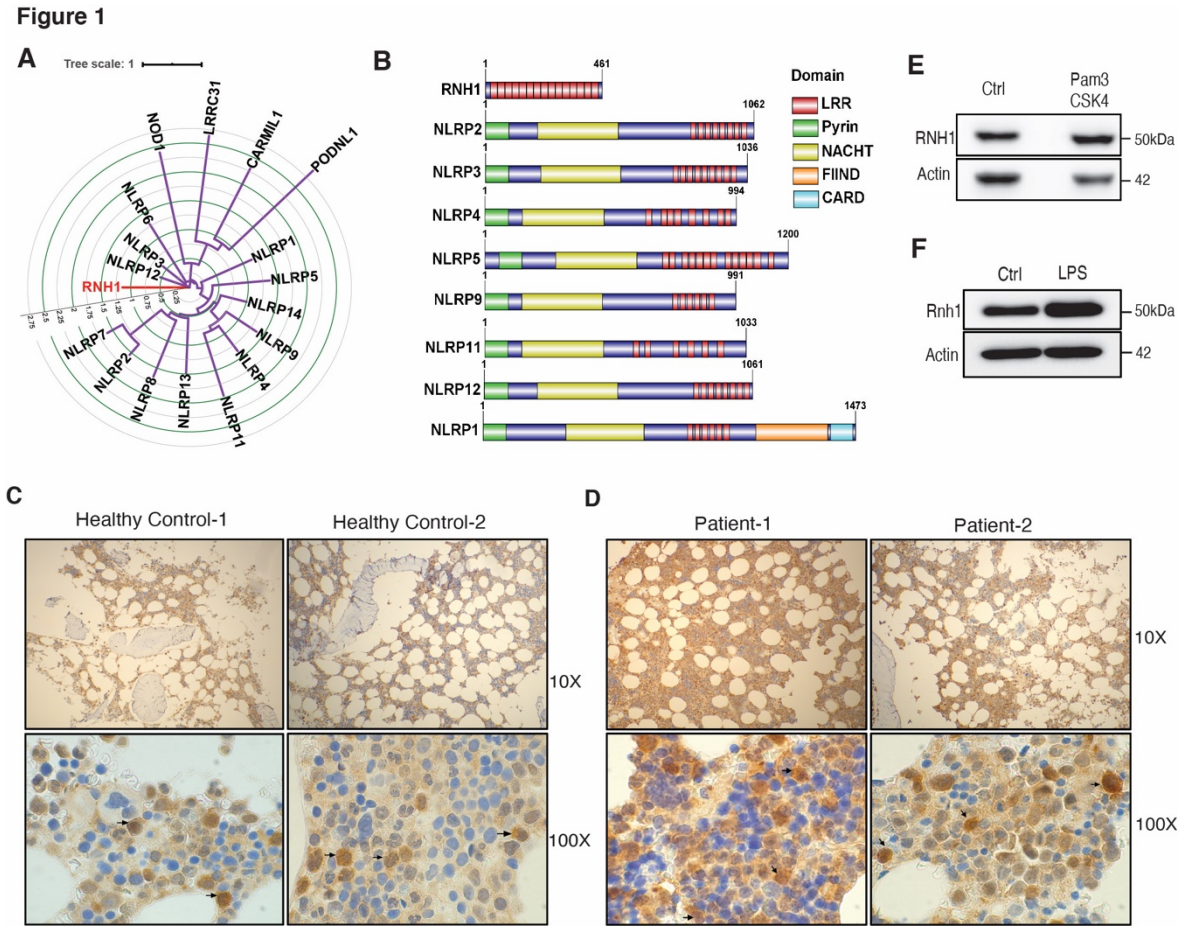

Figure 1. RNH1 shares homology with multiple NLR proteins and is expressed in myeloid cells.

(A) Circular tree representing the domain conservation relationship of human RNH1. Protein sequence alignments were made using MAFFT. A maximum–likelihood phylogenetic tree was generated using IQ-Tree with 1000 bootstrap replicates. Internal tree scale is shown with circular grid.

(**B**) Structural alignment of protein domains. The domain information of selected proteins taken from Uniprot and represented using Illustrator for Biological Sequences (IBS) tool.

(**C**) Human healthy bone marrow biopsies were stained with RNH1 antibody. Myeloid cells showing high RNH1 expression are indicated with arrows. Original magnification 10 X and 100X.

(**D**) Bone marrow biopsies from patients with confirmed inflammatory conditions were stained with RNH1 antibody. Myeloid cells with increased RNH1 expression are indicated with arrows. Original magnification 10X and 100X

(**E**) THP1 cells were stimulated with TLR2 ligand Pam3CSK4 (1 μg/ml) for 24 hours. Total protein lysates were isolated and analyzed by Western blot with indicated antibodies. Blots are representative of two independent experiments.

(**F**) Mouse primary BMDMs were stimulated with TLR4 ligand LPS (1 μg/ml) for 24 hours. Total protein lysates were isolated and analyzed by Western blot with indicated antibodies. Blots are representative of two independent experiments.

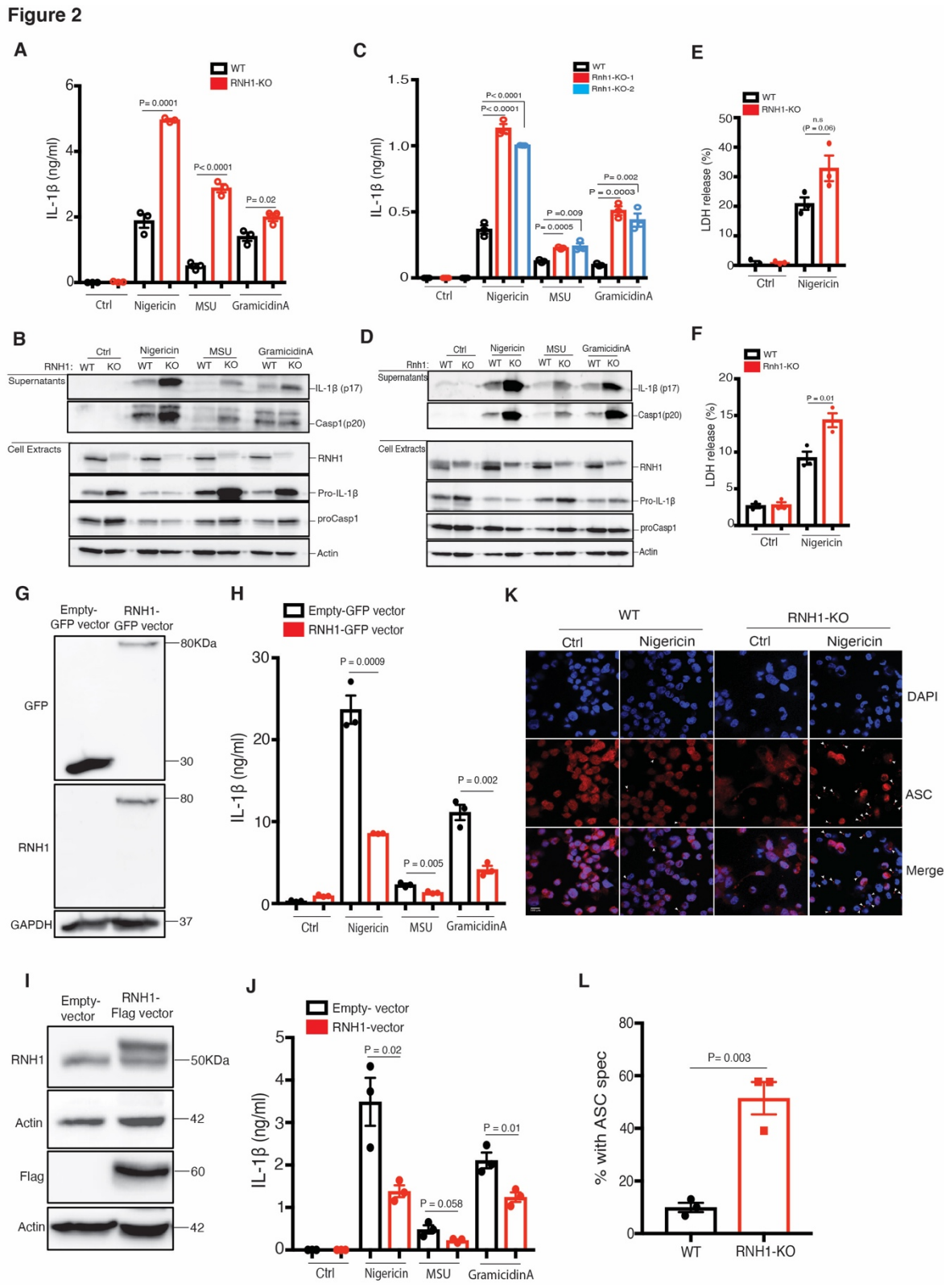

Figure 2. RNH1 inhibits NLRP3 inflammasome activation.

(**A** and **B**) PMA differentiated wildtype and RNH1-KO THP1 cells were stimulated with Nigericin (5 μM) for 1h or with MSU (500 μg) and Gramicidin A (30 μg) for 5h. (A)

Supernatants were collected and IL-1β ELISA was performed. Data are means ± SEM of pooled data from three independent experiments. Statistical analyses were performed using the two-tailed *t*-test. (B) Cell lysates and supernatants were analysed for pro- and cleaved-forms of caspase1 and IL-1β by western blot. Blots were representative of three independent experiments.

(**C** and **D**) Wildtype and Rnh1-KO iMAC cells were primed with 500 ng of LPS for 3h and then stimulated with Nigericin (5μM) for 1h or with MSU (500μg) and Gramicidin A (30μg) for 5h. (C) Supernatant were collected and IL-1β ELISA was performed. Data are means ± SEM of pooled data from three independent experiments. Statistical analyses were performed using the two-tailed *t*-test. (D) Cell lysates and supernatants were analysed for Pro- and cleaved- forms of caspase1 and IL-1β by western blot. Blots were representative of three independent experiments.

(**E**) Wildtype and RNH1-KO THP1 cells were stimulated with NLRP3 agonist Nigericin (5μM) for 18h. Supernatant were collected, and cell death was measured by LDH assay. Data are means ± SEM of pooled data from three independent experiments. Statistical analyses were performed using the two-tailed *t*-test.

(**F**) Wildtype and Rnh1-KO iMAC cells were stimulated with NLRP3 agonist Nigericin (5μM) for 8h. Supernatants were collected, and cell death was measured by LDH assay. Data are means ± SEM of pooled data from three independent experiments. Statistical analyses were performed using the two-tailed *t*-test.

(**G** and **H**) RNH1-KO THP-1 cells transiently infected with GFP tagged control or RNH1 expressing lentivirus particles and cell lysates were analysed by western blot to demonstrate the RNH1 reconstitution in RNH1-KO THP1 cells (G). Blots are representative of three

independent experiments. These cells were stimulated with Nigericin (5 μM) for 1h or with MSU (500 μg) or Gramicidin A (30 μg) for 5h. Supernatant were collected and IL-1β ELISA was performed (H). Data are means ± SEM of pooled data from three independent experiments.

(**I** and **J**) Total cell lysates from THP1 cells constitutively expressing control or Flag-RNH1 were analysed by Western blot with indicated antibodies to demonstrate RNH1 overexpression (I) Blots are representative of three independent experiments. These cells were stimulated with Nigericin (5 μM) for 1h or with MSU (500 μg) or Gramicidin A (30 μg) for 5h. Supernatants were collected and IL-1β ELISA was performed (J). Data are means ± SEM of pooled data from three independent experiments.

(**K** and **L**) Immunofluorescence microscopy analysis of ASC specks in THP1 cells stimulated with Nigericin 5 μM) for 1h. DNA staining is shown in blue (DAPI) and ASC staining is shown in red. Arrowheads indicate ASC inflammasome specks. (Scale bar: 100 μm) (K). Quantification of ASC specks. Data are means ± SEM of pooled data analysing at least 10 fields from three independent experiments.

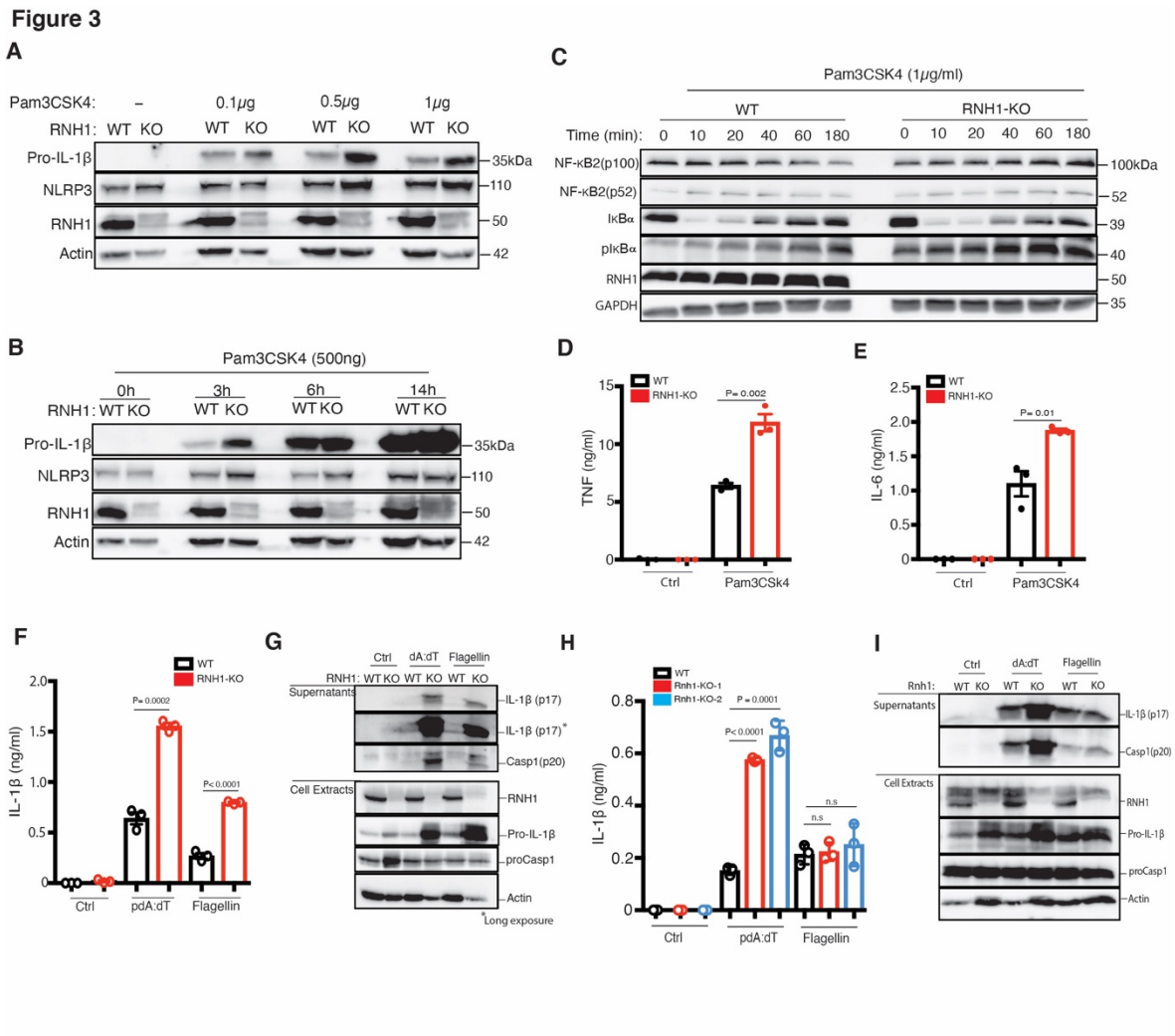

Figure 3. RNH1 negatively regulates activation of NF-κB, AIM2 and NAIP/NLRC4.

(**A** and **B**) Undifferentiated wildtype (WT) and RNH1-KO THP1 cells were stimulated with TLR2 ligand Pam3CSK4 in a dose- (A) and time- (B) dependent manner as indicated. Total cell lysates analysed for pro-IL-1β and NLRP3 expression by Western blot. Blots are representative of three independent experiments.

(**C**) Undifferentiated wildtype and RNH1-KO THP1 cells were stimulated with Pam3CSK4 (1μg/mL) for different time points as indicated. Total cell lysates analysed for NF-κB activation by Western blot with indicated antibodies. Blots are representative of three independent experiments.

(**D** and **E**) Undifferentiated wildtype and RNH1-KO THP1 cells were stimulated with Pam3CSK4 (1µg/mL) for 6h and 18h. Supernatants were analyzed for TNF and IL-6 by ELISA, respectively. Data are means ± SEM of pooled data from three independent experiments.

(**F** and **G**) PMA differentiated wildtype and RNH1-KO THP1 cells were transfected with AIM2 agonist poly dA:dT (5 µg) or NAIP/NLRC4 agonist cytosolic flagellin (600 ng) for 5h. (**F**) Supernatant were collected and IL-1β ELISA was performed. Data are means ± SEM of pooled data from three independent experiments. Statistical analyses were performed using a two-tailed *t*-test. (**G**) Cell lysates and supernatants were analysed for pro- and cleaved- forms of caspase1 and IL-1β by Western blot. Blots are representative of three independent experiments.

(**H** and **I**) iMAC cells were primed with 500 ng of LPS for 3h and then transfected with AIM2 agonist poly dA:dT (5 µg) or NAIP/NLRC4 agonist cytosolic flagellin (600 ng) for 5h. (H) Supernatants were collected and IL-1β ELISA was performed. Data are means ± SEM of pooled data from three independent experiments. Statistical analyses were performed using a two-tailed *t*-test. (I) Cell lysates and supernatants were analysed for pro- and cleaved-forms of caspase1 and IL-1β by Western blot. Blots were representative of three independent experiments.

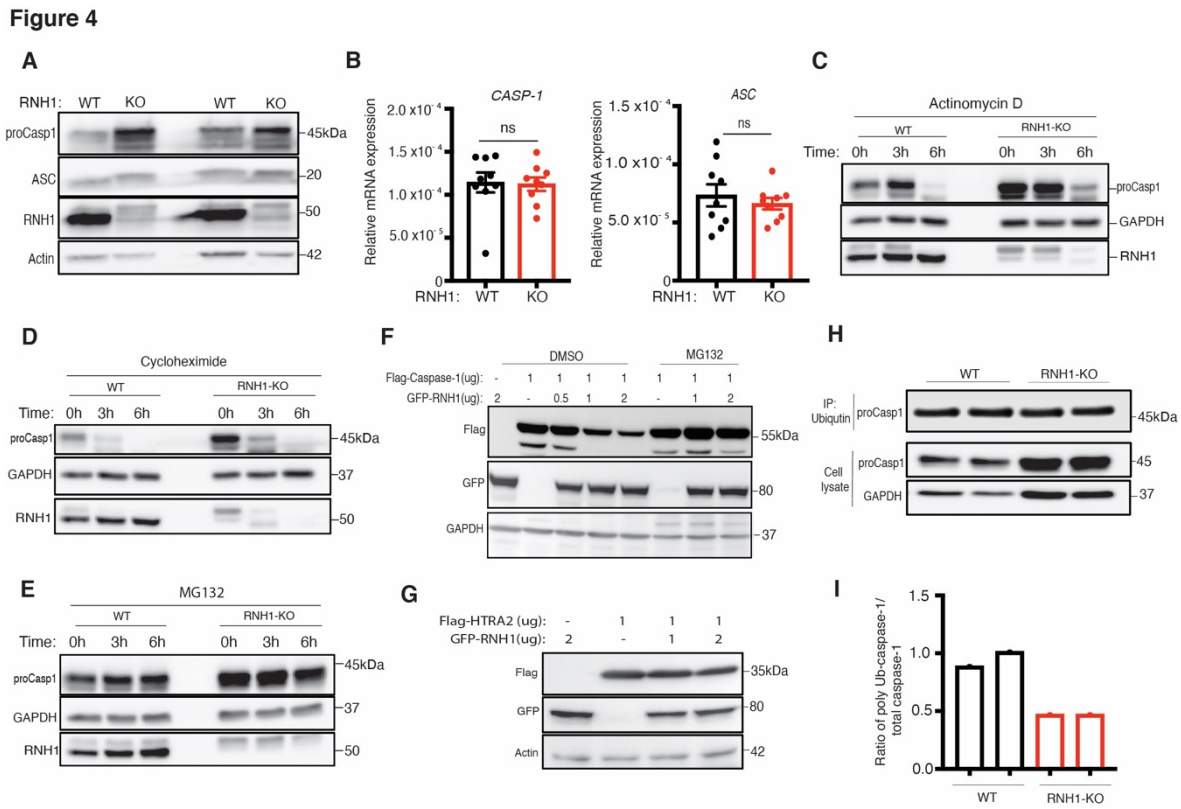

Figure 4. RNH1 increases caspase-1 degradation through the proteosome.

(**A**) Total cell lysates from wildtype and RNH1-KO THP1 cells were analysed for pro-caspase-1 and ASC expression by Western blot. Blots are representative of two independent experiments.

(**B**) qRT-PCR analysis for *CASP-1* and *ASC* mRNAs from wildtype and RNH1-KO THP1 cells. mRNA levels are normalized to 18S rRNA expression. Data shown as means ± SEM and are pooled from three independent experiments

(**C-E**) Wildtype and RNH1-KO THP1 cells were treated with Actinomycin D or Cycloheximide or with the proteasome inhibitor MG-132 for indicated time duration. Cell lysates were analysed for pro-caspase-1 protein levels by Western blot. Blots are representative of three independent experiments.

(**F**) HEK293T cells were treated with or without MG-132 and transfected with Flag-tagged casapase-1 with different concentration of GFP-tagged RNH1 plasmid as indicated. Cells were harvested and cell lysates were analyzed for caspase-1 by Western blot with the indicated antibodies. Blots are representative of three independent experiments.

(**G**) HEK293T cells were transfected with Flag-tagged OMI/HTRA2 plasmid with different concentrations of GFP-tagged RNH1 plasmid as indicated. Cells were harvested and cell lysates were analyzed by Western blot with indicated antibodies. Blots are representative of three independent experiments.

(**H and I**) Whole cell lysates of WT and RNH1-KO THP1 were used for anti-ubiquitin immunoprecipitation and Western blot was performed, as indicated. Blots are representative of three independent experiments (H). Bar graph shows ratio between poly ubiquitin caspase-1 and total caspase-1 levels. Band intensities were calculated by using ImageJ analysis (I).

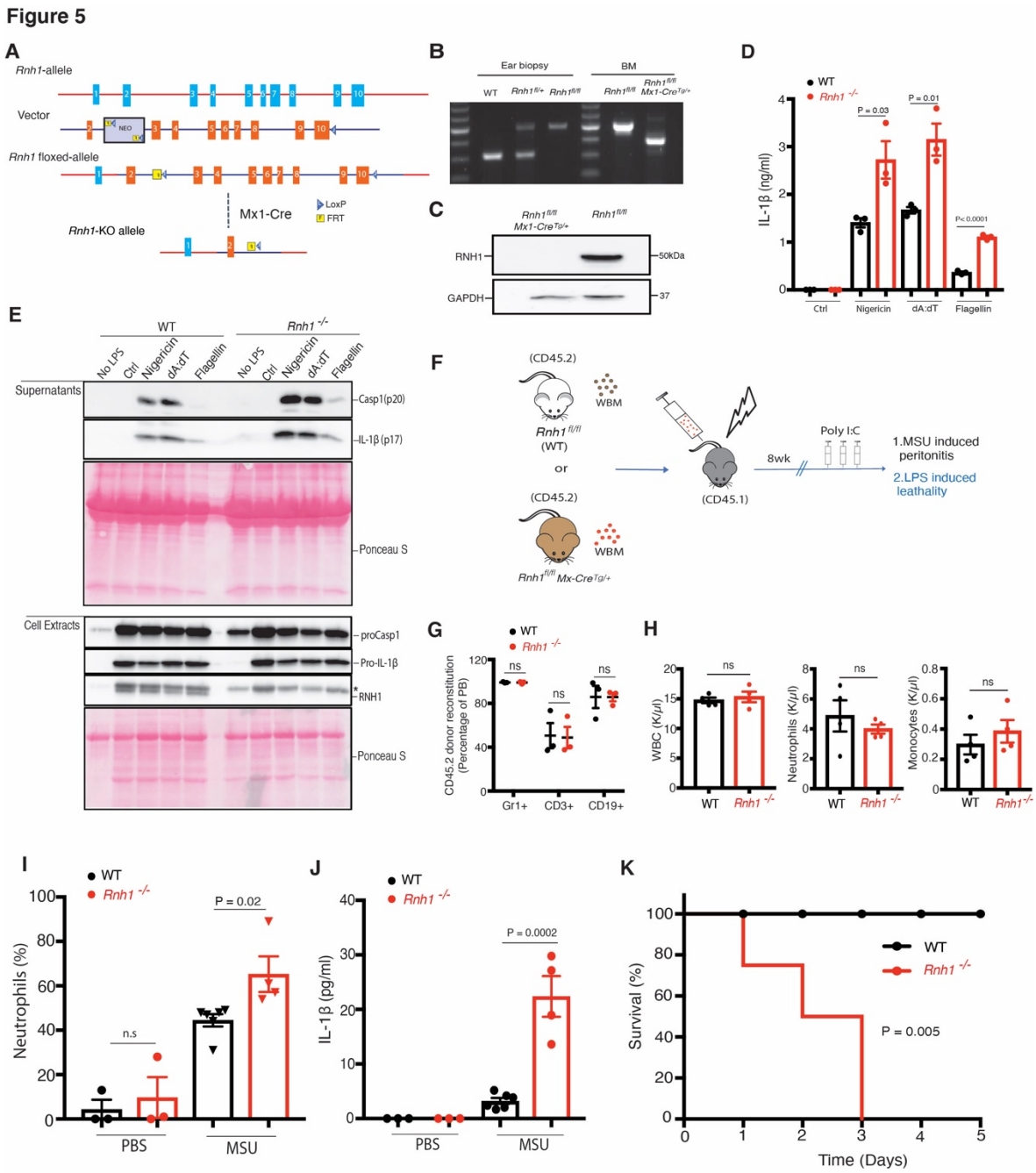

Figure 5. Rnh1 deficiency promotes inflammation in mice.

(A) A 13.8 kb region used to construct the targeting vector was first subcloned from a positively identified C57BL/6 BAC clone (RP23: 217N5) using a homologous recombination-based technique. The region was designed in a way that the long homology arm (LA) extends 6.23 kb 3' to the single LoxP site. The short homology arm (SA) extends about 3.0 kb 5' to the LoxP/FRT flanked Neo cassette. The single LoxP site is inserted

downstream of exon 10, and the Neo cassette is inserted upstream of exon 3. The size of the target region is about 4.6 kb containing exons 3-10.

(**B)** DNA isolated from mouse ear biopsies was genotyped by PCR. Primers were designed to distinguish WT and floxed allele sequence. 314 bp size corresponds to WT, and 514 bp size corresponds to floxed gene. To detect Rnh1 deletion after Cre-recombination in *Rnh1*$^{fl/fl}$ MxCre^{+} mice (after one week of polyIC treatment), a third primer was used which amplifies 365 bp size (see methods)

(C) Total protein lysates from BM cells of WT and *Rnh1*$^{-/-}$ mice were analyzed by Western blot with the indicated antibodies. Blots are representative of 3 independent experiments.

(D and **E**) BMDMs from WT and *Rnh1*$^{-/-}$ mice primed with LPS (100 ng) for 3h and then cells were stimulated with Nigericin (5 μM) for 1h or transfected with poly dA:dT (5 μg) or flagellin (600 ng) for 5h. **(**D) Supernatants were collected and IL-1β ELISA was performed. Data are means ± SEM and representative of three independent experiments. Statistical analyses were performed using a two-tailed *t*-test. (E) Cell lysates and supernatants were analysed for pro- and cleaved- forms of caspase1 and IL-1β by Western blot. Blots were representative of two independent experiments.

(F) Schematic showing *in vivo* experimental setup. Bone marrow was transplanted from wildtype (*Rnh1*$^{fl/fl}$) or *Rnh1*$^{-/-}$ (*Rnh1*$^{fl/fl}$ MxCre^{+}) (CD45.2) into irradiated recipients (CD45.1). After 8 weeks of reconstitution mice were treated with Poly(I:C) (300 μg/mouse) once in two days for three times. Four days later mice were used for the MSU peritonitis and LPS endotoxemia lethality models.

(G) Post transplantation reconstitution levels were monitored after 8 weeks in the peripheral blood (PB) as indicated (n = 3 mice). Data are shown as mean ± SEM. *P* values were determined by 2way ANOVA with Sidak's multiple comparisons test.

(H) PB counts of WBC, neutrophils and monocytes in WT and *Rnh1*$^{-/-}$ mice one week after polyIC injections. Data are shown are mean ± SEM. *P* values were determined by 2-tailed *t*-test (n = 3).

(I and J) WT and *Rnh1*$^{-/-}$ mice received intraperitoneal injection of MSU (1 mg/mouse) or sterile PBS. After 12h, peritoneal lavage fluid was taken and neutrophils infiltration analysed by FACS (I). Peritoneal lavage supernatants were collected and IL-1β levels were quantified by ELISA(J). Data shown as means ± SEM and *P* values were determined by 2-tailed *t*-test (n = 3-6 per group).

(K) Kaplan–Meier survival curves of WT and *Rnh1*$^{-/-}$ mice after LPS (10 mg/kg) treatment (n = 4 mice).

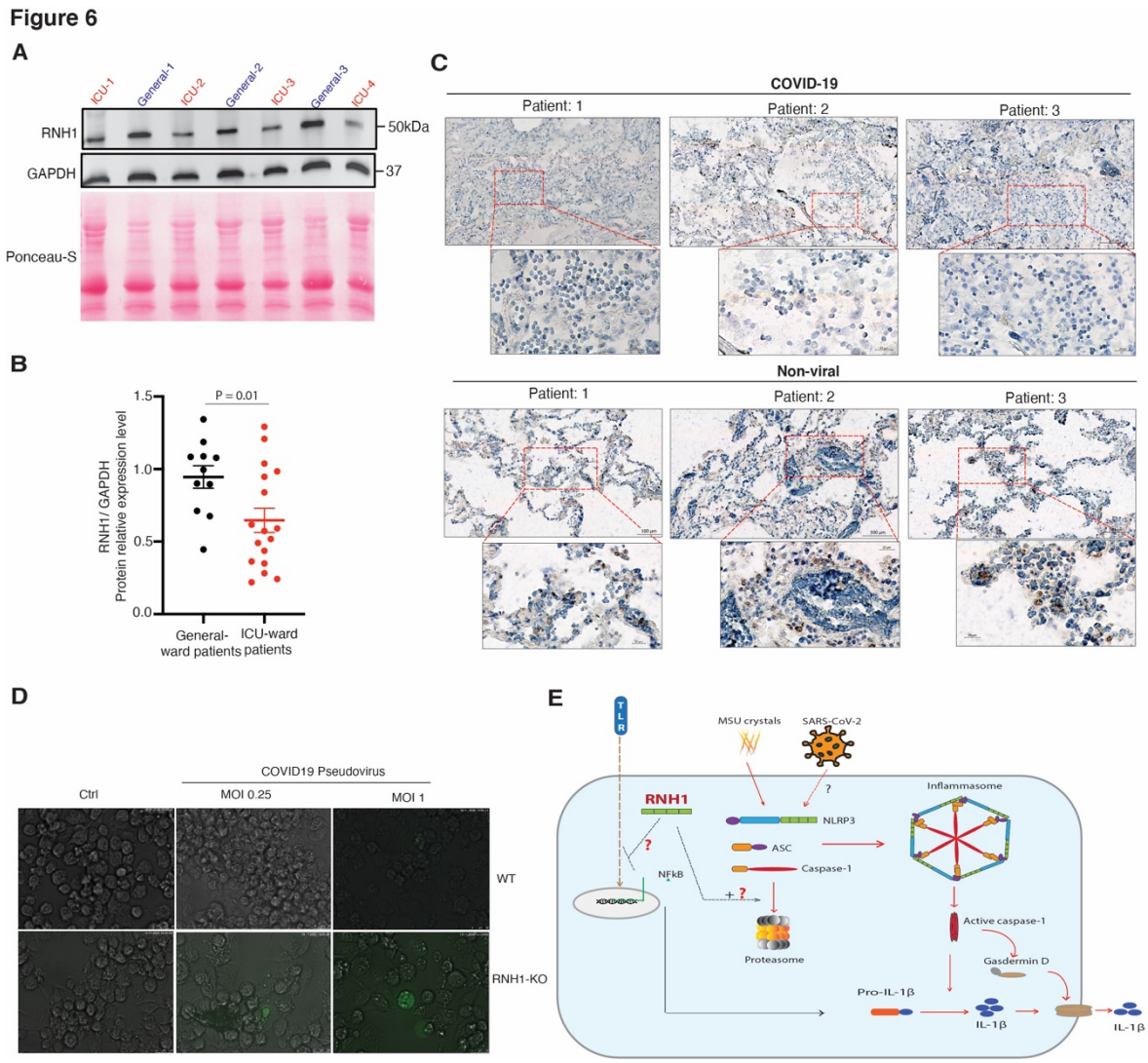

Figure 6. Decrease RNH1 expression correlates with disease severity in COVID-19.

(**A**) Total cell lysates from peripheral blood buffy coats of ICU and general ward admitted COVID-19 patients were analysed for RNH1 protein levels by Western blot. Blots were repeated three times.

(**B**) RNH1 protein levels from blots were quantified by ImageJ analysis for each patient and normalized with respective GAPDH protein levels.

(**C**) Postmortem lung tissue from deceased persons with either COVID-19 or non-viral causes of death were stained for RNH1 and imaged using a Zeiss axioscan Z1. Subsequent image analysis was performed using Zeiss ZEN software to extract images at different

magnifications. Insets show higher magnification of area indicated in the red boxes. Brown staining indicates RNH1 positive cells.

(**D**) PMA differentiated wildtype and RNH1-KO THP1 cells were infected with SARS-CoV-2 pseudovirus for 24 hours. Infection efficiency was monitored by measuring GFP signal with fluorescence microscopy. Images are representative of two independent experiments. (Scale bar 25 µm).

(**E**) Illustration of RNH1 mediated anti-inflammatory mechanisms. First, RNH1 could potentially inhibit NF-kb signaling by unknown mechanism. Second, RNH1 regulates inflammasome activation by controlling caspase-1 protein levels by proteasome-mediated degradation.

MATERIALS AND METHODS

Details of Rnh1 conditional-knockout mice generation and mouse experiments

Rnh1 conditional-knockout (*Rnh1*$^{fl/fl}$) mice were generated on a C57BL/6 background. *Rnh1* targeting vector (**Figure. 5A**) was electroporated into (C57BL/6) embryonic stem (ES) cells. Targeted (C57BL/6 FLP) embryonic stem cells were microinjected into Balb/c blastocysts. Resulting chimeras with a high percentage black coat colour were mated to C57BL/6 WT mice to generate Neo deleted, F1 heterozygous offspring. Germline transmission was confirmed by PCR of tail genomic DNA. Screening of *Rnh1*$^{fl/fl}$ mice by PCR genotyping was

carried out using the following primers on ear genomic DNA: 5'-ACATGGTGTTCTGGG TGTACGGTGG-3' (forward in the intron region after second exon), 5'-CTGAGTAAGGAC TGCTGGGCTGAG-3' (reverse in the proximal *LoxP* region). This reaction amplifies 314 bp in size for WT allele and 514 bp size for floxed allele (**Figure. 5B**).

We crossed *Rnh1*$^{fl/fl}$ mice with *Mx1-Cre* mouse strain (Jackson: 002527) to generate inducible mouse model (*Rnh1*$^{fl/fl}$ *Mx1-Cre*$^{+}$). To exclude non-haematopoietic deletion, total bone marrow (BM) was isolated from wildtype (*Rnh1*$^{fl/fl}$) or *Rnh1*$^{fl/fl}$ *Mx1-Cre*$^{+}$ mice and transplanted (7x10^{6} BM cells) into lethally irradiated CD45.1^{+} congenic recipient mice (8 weeks old male mice) (B6.SJL-*Ptprc*^{a}*Pepc*^{b}/BoyCrl, from Charles river). After 8 weeks of reconstitution, *Rnh1* was excised by giving three rounds of 200 µg poly(I:C) (Invivogen) using intraperitoneal injections once in two days. We used these mice for MSU induced peritonitis model and LPS lethality model. To detect *Rnh1* deletion after Cre-recombination, we used third primer 5'-AAGACCCATCCAGAGCCGAGG-3' (reverse in the distal intron region) in above mentioned PCR reaction using DNA form BM cells, which amplifies 365 bp size (**Figure 5B**) and also western blot was performed in BM cells to check RNH1 protein expression (**Figure 5C).** Mouse peripheral blood was taken from the lateral tail vein with an EDTA coated Microvette 100 K3E (Sarstedt, 20.1278). Full blood counts were measured on an IDEXX ProCyte Dx^{TM} Hematology Analyzer (IDEXX Laboratories). The genotypes of the mice could not be blinded or randomized, due to the experimental design. All groups of mice (experimental and control mice) were age- and sex-matched. We used littermates for our experiments. All animal experiments were approved by the Swiss Federal Veterinary Office (Bern, Switzerland) under valid authorization (BE39/16). Mice were handled according to Swiss Federal Veterinary Office guidelines under valid authorization. Mouse strains are available upon request.

MSU-induced peritonitis model

Mice were injected intraperitoneally (IP) with sterile PBS or MSU (1 mg/mouse) to induce peritonitis. After 12 h mice were euthanized by CO2-asphyxiation and the peritoneal cavity was flushed with sterile PBS. The lavage fluid was centrifuged and supernatants were analyzed by ELISA for IL-1β production and the pelleted cells were analyzed for the influx of neutrophils ($CD45^+$, $Ly\text{-}6G^+$, $CD11b^+$) by BD LSRII flow cytometer (BD Biosciences). Data were analysed by using FlowJo (version 9.3.1, TreeStar Inc) software.

LPS-induced septic shock

Mice were injected intraperitoneally (IP) with LPS (10 mg/kg) or PBS and survival rates were monitored.

Histopathology and bone marrow biopsies

Healthy human controls and inflammatory disease patients bone marrow biopsies were obtained from Swiss MDS Registry. Biopsies were stained with human RNH1 antibody from Prestige Antibodies® Sigma (HPA039223). These studies were approved by the competent local human ethics committee (ID:2017-00734).

Specimen	**Clinical information**
Healthy control 1	Motorcycle accident and bone marrow without specific changes
Healthy control 2	Bicytopenia and splenomegaly, bone marrow morphologically without specific changes
Patient 1	Metastatic Adenocarcinoma of the lungs with inflammation
Patient 2	Suspicion of mastocytosis, bone marrow without specific changes

Cells and cell culture media

Mouse bone marrow derived macrophages (BMDM), iMACs (immortalized macrophages) and Human THP-1 cells were used for inflammasome activation experiments.THP-1 cells and iMACs were grown in RPMI 1640 GlutaMAX™-I medium (Invitrogen) were

supplemented with 10% (vol/vol) FBS (Amimed), 1% of penicillin and streptomycin (PAA Laboratories), at 37 °C and 5% CO_2. BMDMs were generated by established protocols. Briefly, total bone marrow cells were isolated from the femur and tibias of mice and differentiated into macrophages for 7 days in complete DMEM medium (500 mL, ThermoFisher) supplemented with M-CSF (40 ng/mL) (315-02, Peprotech).

Reagents and plasmids

We purchased Nigericin (N7143), pdA:dT (poly(dA-dT)•poly(dT-dA)) sodium salt (P0883), Gramicidin A (G5002) , PMA (P1585), Actinomycin D and Cycloheximide from Sigma-Aldrich, Ultra-pure flagellin (AG-40B-0025) from Adipogen. ultrapure LPS (LPS-EK), MSU (tlrl-msu) and Pam3Cysk4 (tlrl-pms) from Invivogen.

Cloning of Full-length Caspase-1 and OMI were amplified by PCR and sub-cloned into the mammalian expression vectors pCR3 in frame with the N-terminal flag tags. Full-length RNH1-Flag construct was described previously(Chennupati et al., 2018). To construct full length GFP-RNH1 plasmid a human RNH1-full coding sequence (ORIGEN RC 200082) insert was cloned into the entry vector pENTR4-GFP-C1 (W392-1, Addgene) and then recombined into the destination vector pLenti CMV Blast DEST (706-1, Addgene) plasmid, using the Gateway cloning method.

Stimulation Experiments

All cells were stimulated at a density of 1×10^6 cells per ml as describe previously (Allam et al., 2014) Briefly, for inflammasome studies THP1 cells were treated with PMA (100ng/ml) to differentiate into macrophages or BMDMs and iMACs were pre-stimulated for 3 hours with 100 ng/mL of ultrapure LPS. Later cells were stimulated with 1 hour with 5uM of Nigericin or 5µg/mL of pdA:dT, 30µg/mL of Gramicidin A, 300µg/mL MSU and 200ng/mL of Flagellin. pdA:dT and flagellin were transfected with Lipofectamine 2000 according to

the manufacturer's protocol (Invitrogen). For all conditions, cell-free supernatants were analyzed by ELISA for cytokine secretion or cells were lysed for immunoblot analysis.

CRISPR/CAS9-mediated RNH1-knockout THP1 and iMAC cell line generation

RNH1-KO THP1 cells (human monocytic cell line) were generated as described previously (Chennupati et al., 2018). For RNH1-KO iMAC cells CRISPR sequences targeting exon 2 (RNH1-KO-1) and exon 3 (RNH1-KO-2) of mouse RNH1 were designed and obtained KO cells as described previously. Target exon and the seed sequences preceding the protospacer adjacent motif (PAM) are the following: RNH1-1 oligo 1- 5′-*CACC*GTCTGA TCCAGCAATACGAAG-*3'*; RNH1-1oligo 2— 5′-AAACCTTCGTATTGCTGGA TCAGAC-3′; RNH1-2 oligo 1- 5′-*CACC*GGATAACCCTATGGGGGACG*C-3 '*; RNH1-2 oligo 2- 5′-AAACGCGTCCCCCATAGGGTTATCC-3'. All the generated THP1 and iMAC clones were tested negative for mycoplasma contamination using MycoAlert Mycoplasma Detection Kit (Lonza, Cat#LT07-318). THP1 cells were obtained from ATCC and iMAC cells were provided by Petr Broz (University of Lausanne).

Generation of stable THP1 cells expressing Flag–RNH1

Flag-RNH1 was further sub cloned into retroviral vector pMSCVpuro (Clontech). Retroviral vector pMSCVpuro-Flag–RNH1 was co-transfected with the helper plasmids VSV-G and Hit60 into HEK293T cells using PEI transfection reagent. Culture supernatants containing recombinant viral particles were harvested and used to infect THP1 cells. To establish stable cell lines, THP1 cells were selected with puromycin (5ug ml^{-1}) 3 days after infection.

Generation of transient THP1 cells expressing GFP–RNH1

RNH1-KO THP1 cells were infected with lentiviruses expressing RNH1 (pLenti CMV Blast GFP- RNH1) or the empty vector pLentiCMV-GFP-Blast (659-1, Addgene) as previously described (Papin et al., 2007). After 48 h post-infection, efficiency was monitored by GFP

expression and blasticidin (5μg/mL) selected THP1 cells were plated for inflammasome assay.

Generation of stable THP1 cells expressing shRNA-RNH1

Various lentiviral shRNA plasmids against RNH1 were purchased from Sigma. THP1 cells stably expressing shRNA were obtained as previously described.

Immunoblot analysis

Precipitated media supernatants or cell extracts were analyzed by standard immunoblot techniques. The following antibody were used. Anti-human RNH1 (A9), anti-mouse RNH1 (C10), anti-human ASC (Sc-514414), anti-GAPDH (G9, sc-365062) from Santa Cruz Biotechnology. Anti- human IL-1β antibody (12242), anti-NFκB2 (p100), anti-IκBα, anti-Phospho-IκBα, anti-GFP (2555) from Cell signalling. Anti-human Caspase-1 (p20, Bally-1), anti-mouse Caspase-1 (p20, AG-20B-0042), anti-NLRP3 (Cryo-2), anti-mouse ASC (AG-25B-0006) from Adipogen. Anti-mouse IL-1β antibody (AF-401-NA) from R&D. Anti-β-Actin from Abcam.

TLR priming and NF-κB activation

Wildtype and RNH1-KOTHP1 cells were stimulated with TLR2 agonist Pam3CSK4 (500ng/mL) at different time points 3, 6 and 14h or at different doses 100, 500 and 1000 ng/mL for 3h. For NF-*κB* activation, cells were stimulated at 10, 20, 40, 60 and 180 minutes by Pam3CSK4 (1000 ng/mL). After stimulation cell lysates were isolated and performed Western blot.

Caspase-1 expression and ubiquitination

HEK293T cells were treated with or without MG-132 and transfected with full length flag-tagged Casapase-1 or OMI/HTAR2 plasmids with or without GFP-tagged RNH1 plasmid as indicated concentration. At 24 hour, cells were harvested and cell lysates were analyzed by immunoblot. To check the caspase-1 ubiquitination, WT and RNH1-KO THP1 cells were

resuspended in lysis buffer (20 mM Tris, pH 7.4, 150 mM NaCl, 1% [vol/vol] Nonidet-P40, 10 mM EDTA). Using these whole cell lysates, immuno- precipitation was performed with Ubiquitin antibody (Sc-8017, Santa Cruz Biotechnology) bound to Dynabeads Protein G (10003D, Life Technologies) for 3 hours with rotation at 4°C. Immunoprecipitated proteins were washed in lysis buffer, eluted, resolved by SDS-PAGE and detected by immunoblot analysis.

Cytokine measurement and LDH assay

Cell supernatants were analyzed for cytokines and Lactate Dehydrogenase (LDH). Human and mouse IL-1β, TNF and IL-6 cytokine secretion measured by ELISA according to the manufacturer's instructions (eBioscience). LDH was measured by colorimetric NAD linked assay by in-house developed kit according OPS Diagnostics instructions.

Detection of ASC oligomerization by western blot

We detected ASC oligomerization by western blot as described previously (Lugrin and Martinon, 2017). Briefly, WT and RNH1-KO THP1 cells were primed with 100 ng of PMA and treated with Nigericin (5 µM) for 1 hour and Poly(dA:dT) (5 µg), for 5 hours. After stimulation, cells were detached and lysed on ice cold lysis buffer (20 mM Hepes·KOH, pH 7.5, 10 mM KCl, 1.5 mM MgCl2, 1 mM EDTA, 1 mM EGTA and 320 mM sucrose) by syringing 35 times using a 21G needle. Cell lysates were centrifuged for 8 min at 1,800 *x g* and supernatants were collected (30 µL of the supernatants were kept aside to check ASC expression in the lysates). Supernatants were further diluted two times with lysis buffer and then centrifuged at 2,000 *x g* for 5 min. Next, supernatants were diluted with 1 vol of CHAPS buffer (20 mM Hepes·KOH, pH 7.5, 5 mM MgCl2, 0.5 mM EGTA, 0.1 mM PMSF and 0.1% CHAPS) and then centrifuged for 8 min at 5,000 *x g*. The supernatant was discarded and the pellet was resuspended in 50µL of CHAPS buffer supplemented with 4mM of

disuccinimidyl suberate (Thermo Scientific) and incubated at room temperature for 30 min. After incubation, samples were centrifuged for 8 min at 5,000 *x g*, and pellets were resuspended in SDS sample buffer without reducing agents and western blot was performed.

Detection of ASC Spec formation by confocal microscopy

To further confirm the ASC specks formation, we performed confocal microscopy as described previously (Di Micco et al., 2016). Briefly, PMA-primed WT and RNH1-KO THP1 cells were seeded on coverslips in 12-well plates before inflammasome activation. Next day, cells were stimulated for 1h with Nigericin (5 µM) and fixed with 4% (vol/vol) PFA (Applichem) for 20 min at room temperature (RT). After fixation, cells were washed 3 times with 1x PBS for 5 min and permeabilize with 0.1% Triton X-100 in 1x PBS for 15 min at RT. Cell were washed with 1x PBS and blocked with 4%(w/vol) BSA for 30 min at RT. After blocking, cells were incubated overnight at 4 °C with the primary antibodies against ASC (HASC-71, BioLegend). Cells were washed 3 times with washing buffer (1x PBS and 0.025% of Tween20) for 5 min and incubated for 1h at RT with the Alexa Fluor secondary antibodies (Thermo Scientific). Cells were washed twice with washing buffer for 5 min and incubated in with DAPI (1 µg/mL) for 1 min. Again, cells were washed and coverslips were mounted on glass slides using mounting media (ProLong® Gold Antifade). Images were captured with inverted confocal microscope LSM 710 (Zeiss) and analyzed with ImageJ across at least 10 fields from three independent experiments.

Actinomycin D, Cycloheximide and MG-132 chase assays

To study Caspase-1 mRNA and protein stability, wildtype and RNH1-KO THP1 cells were treated with the following inhibitor 3 and 6 Hours. Cell were treated with Actinomycin D (10 µg/mL), Cycloheximide (75 µg/mL), proteasomal inhibitor MG-132 (20 µM) to assess

transcriptional, translational and posttranslational changes. After treatment, cells were harvested and cell lysates were analyzed by immunoblot.

RNA preparation and qRT-PCR.

Total RNA was isolated from wild type and RNH1-KO THP1 cells using the QIAGEN RNeasy Kit according to the manufacturer's protocol. Complementary DNA was generated from total RNA as described previously (Allam et al., 2015). The SYBR Green Dye detection system was used for quantitative real-time PCR on Light Cycler 480 (RocheControls consisting of ddH_2O were negative for target and housekeeping genes. The following Gene-specific primers (Microsynth) were used. 18SrRNA:5′-GCAATTATTCCCCATGAACG-3′(f), 5′-AGGGCCTCACTAAACCATCC-3′ (r); ASC: 5'-CCT CAG TCG GCA GCC AAG-3' (f), 5'-CAG CAG CCA CTC AAC GTT TG-3' (r); CASP1: 5'-TCC TCA GGC TCA GAA GGG AA-3' (f), 5'-TGC GGC TTG ACT TGT CCA T-3' (r); RNH1: 5'- GATCTGGGAGTGTGGCATCA-3' (f), 5'-CTGCAGGACTTCACCCACAG- 3' (r).

COVID-19 pseudovirus infection

The SARS-CoV-2 pseudoviral particles expressing COVID-19 spike protein pGBW m4137384: S protein was purchased from Addgene (149543) and the virus particles were produced as describe previously (Hoffmann et al., 2020; Nie et al., 2020) .Wildtype and RNH1-KO THP1 cells were treated with PMA (100 ng/mL) to differentiate into macrophages and infected with SARS-CoV-2 pseudovirus at MOI of 20 and 100 for 24 hours. Infection efficiency was monitored by measuring GFP signal using fluorescent microscope (Leica DMI 400 B).

COVID-19 patient samples

We analysed a total of 28 COVID-19 patients samples from a previously published study (n= 13) (Spinetti et al., 2020), but with addition of new patients to the cohort (n=15). We isolated protein samples from buffy coats of COVID-19 patients and analysed RNH1 expression by Western blot. The present study is part of a larger COVID-project (NCT04510012) and data of some patients were previously investigated regarding immune functionality in COVID-19 (Spinetti et al., 2020). The study was performed in accordance with the "Declaration of Helsinki" and approved by the Kantonale Ethikkommission KEK, Bern, Switzerland, Nr. 2020-00877.

COVID-19 Tissue microarray samples

Post-mortem tissues were collected as part of the ethically approved LoST-SoCC study in accordance with the "Declaration of Helsinki" and Human Tissue Authority legislation. The study was approved by the Newcastle North Tyneside 1 research ethics commits 19/NE/0336, IRAS 193937. Non-COVID causes of death were all non-respiratory, non-infectious, obtained from PMs that were done prior to the pandemic and the lungs were morphologically within normal limits. The original FFPE tissue blocks were taken from representative samples at post-mortem, formalin fixed and processed as per standard diagnostic blocks. For tissue microarray (TMA) construction, representative 3mm tissue cores were cored out of FFPE tissue blocks and re-blocked within a 4x4 format TMA, sectioned and mounted onto glass slides.Slides were dehydrated and endogenous peroxides quenched. Antigen retrieval done using TRIS buffer pH9 boiled for 15 minutes. Slides were incubated with permeabilization buffer (0.3% Triton-X100 in PBS) then blocking buffer (10% FBS in PBS). Anti-RNH1 (Prestige Antibodies® Sigma, HPA039223) was added overnight at 1:500, followed by anti-rabbit secondary, ABC amplification and DAB detection (both ThermoFisher). Slides were then counterstained with Meyer's haematoxylin

and coverslips applied with aqueous mounting agent and slides imaged using Zeiss axioscan Z1. Images were analysed using Zen Lite software (Zeiss).

Sequence conservation analysis

Human RNH1 protein sequence was used as a query to perform Blastp with human refseq proteins. From Blast output, selected protein sequences (excluding the isoforms and model refseq proteins) were aligned using MAFFT multiple sequence aligner (Katoh and Standley, 2013). Sequence conservation analysis was performed on IQ-Tree webserver (http://iqtree.cibiv.univie.ac.at/) using ultrafast bootstrap analysis with 1,000 number of bootstrap alignments (Katoh and Standley, 2013) Circular tree was visualized using Interactive Tree Of Life (iTOL) (Letunic and Bork, 2019). For structural alignment of protein domains, the domain information of selected proteins were taken from Uniprot and represented using Illustrator for Biological Sequences (IBS) tool (Liu et al., 2015) Sequences used for multiple sequence alignment: NP_002930.2_RNH1; NP_653288.1_NLRP12; NP_789792.1_NLRP14; NP_703148.4_NLRP5; NP_001120933.2_NLRP3; NP_659444.2_NLRP11; NP_789790.2_NLRP9; NP_001167553.1_NLRP2; NP_604393.2_NLRP4; NP_789780.2_NLRP13; NP_001120727.1_NLRP7; NP_789781.2_NLRP8; NP_127497.1_NLRP1; NP_001264057.1_LRRC31; NP_001263629.1_NLRP6; NP_006083.1_NOD1; NP_079101.4_PODNL1; NP_060110.4_CARMIL1

Statistical analysis

Data were expressed as mean ± SEM. Comparison between two groups was performed by two-tailed *t*-test. A value of $p<0.05$ was considered to be statistically significant. All statistical analyses were calculated using Graph Pad Prism version 8.

Materials Availability

Plamisds and transgenic mice are available upon request. Please contact lead contact :

allam.ramanjaneyulu@dbmr.unibe.ch

REFERENCES

Allam, R., Lawlor, K.E., Yu, E.C.W., Mildenhall, A.L., Moujalled, D.M., Lewis, R.S., Ke, F., Mason, K.D., White, M.J., Stacey, K.J., et al. (2014). Mitochondrial apoptosis is dispensable for NLRP3 inflammasome activation but non-apoptotic caspase-8 is required for inflammasome priming. *15*, 982–990.

Allam, R., Maillard, M.H., Tardivel, A., Chennupati, V., Bega, H., Yu, C.W., Velin, D., Schneider, P., and Maslowski, K.M. (2015). Epithelial NAIPs protect against colonic tumorigenesis. Journal of Experimental Medicine *212*, 369–383.

Arthur, J.S.C., and Ley, S.C. (2013). Mitogen-activated protein kinases in innate immunity. Nature Publishing Group 1–14.

Broz, P., and Dixit, V.M. (2016). Inflammasomes: mechanism of assembly, regulation and signalling. Nat. Rev. Immunol. 1–14.

Chennupati, V., Veiga, D.F., Maslowski, K.M., Andina, N., Tardivel, A., Yu, E.C.-W., Stilinovic, M., Simillion, C., Duchosal, M.A., Quadroni, M., et al. (2018). Ribonuclease inhibitor 1 regulates erythropoiesis by controlling GATA1 translation. J. Clin. Invest. *128*.

Desai, N., Neyaz, A., Szabolcs, A., Shih, A.R., Chen, J.H., Thapar, V., Nieman, L.T., Solovyov, A., Mehta, A., Lieb, D.J., et al. (2020). Temporal and spatial heterogeneity of host response to SARS-CoV-2 pulmonary infection. Nature Communications 1–15.

Di Micco, A., Frera, G., Lugrin, J., Jamilloux, Y., Hsu, E.-T., Tardivel, A., De Gassart, A., Zaffalon, L., Bujisic, B., Siegert, S., et al. (2016). AIM2 inflammasome is activated by pharmacological disruption of nuclear envelope integrity. Proceedings of the National Academy of Sciences *113*, E4671–E4680.

Dickson, K.A., Haigis, M.C., and Raines, R.T. (2005). Ribonuclease inhibitor: structure and function. Prog. Nucleic Acid Res. Mol. Biol. *80*, 349–374.

Druilhe, A., Srinivasula, S.M., Razmara, M., Ahmad, M., and Alnemri, E.S. (2001). Regulation of IL-1beta generation by Pseudo-ICE and ICEBERG, two dominant negative caspase recruitment domain proteins. Cell Death Differ. *8*, 649–657.

Ferreira, A.C., Soares, V.C., Azevedo-Quintanilha, I.G., da Silva Gomes Dias, S., Fintelman-Rodrigues, N., Sacramento, C.Q., Mattos, M., Freitas, C.S., Temerozo, J.R., Teixeira, L., et al. (2021). SARS-CoV-2 engages inflammasome and pyroptosis in human primary monocytes. Cell Death Discovery 1–12.

Furia, A., Moscato, M., Calì, G., Pizzo, E., Confalone, E., Amoroso, M.R., Esposito, F., Nitsch, L., and D'Alessio, G. (2011). The ribonuclease/angiogenin inhibitor is also present in mitochondria and nuclei. FEBS Lett. *585*, 613–617.

Gong, T., Liu, L., Jiang, W., and Zhou, R. (2020). DAMP-sensing receptors in sterile inflammation and inflammatory diseases. Nat. Rev. Immunol. 1–18.

Haigis, M.C., Haag, E.S., and Raines, R.T. (2002). Evolution of ribonuclease inhibitor by exon duplication. Mol. Biol. Evol. *19*, 959–963.

Henao-Mejia, J., Elinav, E., Thaiss, C.A., and Flavell, R.A. (2014). Inflammasomes and metabolic disease. Annu. Rev. Physiol. *76*, 57–78.

Hoss, F., Mueller, J.L., Ringeling, F.R., Rodriguez-Alcazar, J.F., Brinkschulte, R., Seifert, G., Stahl, R., Broderick, L., Putnam, C.D., Kolodner, R.D., et al. (2019). Alternative splicing regulates stochastic NLRP3 activity. Nature Communications 1–13.

Huang, C., Wang, Y., Li, X., Ren, L., Zhao, J., Hu, Y., Zhang, L., Fan, G., Xu, J., Gu, X., et al. (2020a). Clinical features of patients infected with 2019 novel coronavirus in Wuhan, China. Lancet *395*, 497–506.

Huang, Q., Wu, X., Zheng, X., Luo, S., Xu, S., and Weng, J. (2020b). Targeting inflammation and cytokine storm in COVID-19. Pharmacol Res *159*, 105051.

Jin, J., Yu, Q., Han, C., Hu, X., Xu, S., Wang, Q., Wang, J., Li, N., and Cao, X. (1AD). LRRFIP2 negatively regulates NLRP3 inflammasome activation in macrophages by promoting Flightless-I-mediated caspase-1 inhibition. Nature Communications *4*, 1–8.

Jose, R.J., and Manuel, A. (2020). COVID-19 cytokine storm: the interplay between inflammation and coagulation. The Lancet Respiratory *8*, e46–e47.

Katoh, K., and Standley, D.M. (2013). MAFFT multiple sequence alignment software version 7: improvements in performance and usability. Mol. Biol. Evol. *30*, 772–780.

Kobe, B., and Deisenhofer, J. (1993). Crystal structure of porcine ribonuclease inhibitor, a protein with leucine-rich repeats. Nature *366*, 751–756.

Kobe, B., and Kajava, A.V. (2001). The leucine-rich repeat as a protein recognition motif. Curr. Opin. Struct. Biol. *11*, 725–732.

Kroemer, A., Khan, K., Plassmeyer, M., Alpan, O., Haseeb, M.A., Gupta, R., and Fishbein, T.M. (2020). Inflammasome activation and pyroptosis in lymphopenic liver patients with COVID-19. J Hepatol *73*, 1258–1262.

Kühn, R., Schwenk, F., Aguet, M., and Rajewsky, K. (1995). Inducible gene targeting in mice. Science *269*, 1427–1429.

Lamkanfi, M., and Dixit, V.M. (2011). Inflammasomes and Their Roles in Health and Disease. Annu. Rev. Cell Dev. Biol. *28*, 120913150209003.

Latz, E., Xiao, T.S., and Stutz, A. (2013). Activation and regulation of the inflammasomes. Nat. Rev. Immunol. *13*, 397–411.

Letunic, I., and Bork, P. (2019). Interactive Tree Of Life (iTOL) v4: recent updates and new developments. Nucleic Acids Res. *47*, W256–W259.

Li, J., Yin, H.L., and Yuan, J. (2008). Flightless-I regulates proinflammatory caspases by selectively modulating intracellular localization and caspase activity. J. Cell Biol. *181*, 321–333.

Li, P., Allen, H., Banerjee, S., Franklin, S., Herzog, L., Johnston, C., McDowell, J., Paskind, M., Rodman, L., and Salfeld, J. (1995). Mice deficient in IL-1 beta-converting enzyme are defective in production of mature IL-1 beta and resistant to endotoxic shock. Cell *80*, 401–411.

Liu, W., Xie, Y., Ma, J., Luo, X., Nie, P., Zuo, Z., Lahrmann, U., Zhao, Q., Zheng, Y., Zhao, Y., et al. (2015). IBS: an illustrator for the presentation and visualization of biological sequences. Bioinformatics *31*, 3359–3361.

Lucas, C., Wong, P., Klein, J., Castro, T.B.R., Silva, J., Sundaram, M., Ellingson, M.K., Mao, T., Oh, J.E., Israelow, B., et al. (2020). Longitudinal analyses reveal immunological misfiring in severe COVID-19. Nature 1–25.

Lugrin, J., and Martinon, F. (2017). Detection of ASC Oligomerization by Western Blotting. Bio Protoc *7*, e2292–e2292.

Man, S.M., Karki, R., Briard, B., Burton, A., Gingras, S., Pelletier, S., and Kanneganti, T.-D. (2017). Differential roles of caspase-1 and caspase-11 in infection and inflammation. Nature Publishing Group 1–11.

Martinon, F., Mayor, A., and Tschopp, J. (2009). The inflammasomes: guardians of the body. Annu. Rev. Immunol. *27*, 229–265.

Martinon, F., Pétrilli, V., Mayor, A., Tardivel, A., and Tschopp, J. (2006). Gout-associated uric acid crystals activate the NALP3 inflammasome. Nature *440*, 237–241.

Matsushima, N., Miyashita, H., Mikami, T., and Kuroki, Y. (2010). A nested leucine rich repeat (LRR) domain: the precursor of LRRs is a ten or eleven residue motif. BMC Microbiol *10*, 235–10.

Mehta, P., McAuley, D.F., Brown, M., Sanchez, E., Tattersall, R.S., Manson, J.J., and HLH Across Speciality Collaboration, U.K. (2020). COVID-19: consider cytokine storm syndromes and immunosuppression. The Lancet *395*, 1033–1034.

Miao, E.A., Rajan, J.V., and Aderem, A. (2011). Caspase-1-induced pyroptotic cell death. Immunol. Rev. *243*, 206–214.

Monti, D.M., Montesano Gesualdi, N., Matousek, J., Esposito, F., and D'Alessio, G. (2007). The cytosolic ribonuclease inhibitor contributes to intracellular redox homeostasis. FEBS Lett. *581*, 930–934.

Ng, A.C.Y., Eisenberg, J.M., Heath, R.J.W., Huett, A., Robinson, C.M., Nau, G.J., and Xavier, R.J. (2011). Human leucine-rich repeat proteins: a genome-wide bioinformatic categorization and functional analysis in innate immunity. Proc. Natl. Acad. Sci. U.S.a. *108 Suppl 1*, 4631–4638.

Papin, S., Cuenin, S., Agostini, L., Martinon, F., Werner, S., Beer, H.-D., Grütter, C., Grütter, M., and Tschopp, J. (2007). The SPRY domain of Pyrin, mutated in familial Mediterranean fever patients, interacts with inflammasome components and inhibits proIL-1beta processing. Cell Death Differ. *14*, 1457–1466.

Pedraza-Alva, G., Pérez-Martínez, L., Valdez-Hernández, L., Meza-Sosa, K.F., and Ando-Kuri, M. (2015). Negative regulation of the inflammasome: keeping inflammation under control. Immunol. Rev. *265*, 231–257.

Rodrigues, T.S., de Sá, K.S.G., Ishimoto, A.Y., Becerra, A., Oliveira, S., Almeida, L., Goncalves, A.V., Perucello, D.B., Andrade, W.A., Castro, R., et al. (2021). Inflammasomes are activated in response to SARS-CoV-2 infection and are associated with COVID-19 severity in patients. Journal of Experimental Medicine *218*.

Schroder, K., and Tschopp, J. (2010). The Inflammasomes. Cell *140*, 821–832.

Spinetti, T., Hirzel, C., Fux, M., Walti, L.N., Schober, P., Stueber, F., Luedi, M.M., and Schefold, J.C. (2020). Reduced Monocytic Human Leukocyte Antigen-DR Expression Indicates Immunosuppression in Critically Ill COVID-19 Patients. Anesthesia & Analgesia *131*, 993–999.

Strowig, T., Henao-Mejia, J., Elinav, E., and Flavell, R. (2012). Inflammasomes in health and disease. Nature *481*, 278–286.

Stutz, A., Horvath, G.L., Monks, B.G., and Latz, E. (2013). ASC speck formation as a readout for inflammasome activation. Methods Mol. Biol. *1040*, 91–101.

Tavernier, Q., Bennana, E., Poindessous, V., Schaeffer, C., Rampoldi, L., Pietrancosta, N., and Pallet, N. (2018). Regulation of IRE1 RNase activity by the Ribonuclease inhibitor 1 (RNH1). Cell Cycle *17*, 1901–1916.

Toldo, S., Bussani, R., Nuzzi, V., Bonaventura, A., Mauro, A.G., Cannatà, A., Pillappa, R., Sinagra, G., Nana-Sinkam, P., Sime, P., et al. (2020). Inflammasome formation in the lungs of patients with fatal COVID-19. Inflamm. Res. 1–4.

van den Berg, D.F., and Velde, Te, A.A. (2020). Severe COVID-19: NLRP3 Inflammasome Dysregulated. Front Immunol *11*, 1580.

Vande Walle, L., Lamkanfi, M., and Vandenabeele, P. (2008). The mitochondrial serine protease HtrA2/Omi: an overview. Cell Death Differ. *15*, 453–460.

Yamasaki, S., Ivanov, P., Hu, G.-F., and Anderson, P. (2009). Angiogenin cleaves tRNA and promotes stress-induced translational repression. J. Cell Biol. *185*, 35–42.

Zhu, Y., Das, K., Wu, J., Lee, M.H., and Tan, P. (2013). RNH1 regulation of reactive oxygen species contributes to histone deacetylase inhibitor resistance in gastric cancer cells. Oncogene.